Subfemtosecond glory hologrammetry for vectorial optical waveform reconstruction

J. F. Tao,[1] J. Cai,[2] Q. Z. Xia,[3,*] and J. Liu[4,5,†]

[1]*Beijing Computational Science Research Center, Beijing 100193, China*

[2]*School of Physics and Electronic Engineering, Jiangsu Normal University, Xuzhou 221116, China*

[3]*National Laboratory of Science and Technology on Computational Physics, Institute of Applied Physics and Computational Mathematics, Beijing 100088, China*

[4]*Graduate School of China Academy of Engineering Physics, Beijing 100193, China*

[5]*CAPT, HEDPS, and IFSA Collaborative Innovation Center of MoE, Peking University, Beijing 100871, China*

(Received 4 November 2019; accepted 27 March 2020; published 27 April 2020)

In this work, we propose a method to characterize the temporal structure of arbitrary optical laser pulses with low pulse energies. Our theory is based on strong-field photoelectron holography with the glory rescattering effect as the underlying mechanism in the near-forward direction. Utilizing the subfemtosecond glory rescattering process as a fast temporal gate to sample the unknown light pulse, the time-dependent vectorial electric field can be retrieved from the streaking photoelectron momentum spectra. Our method avoids the challenging task of generation or manipulation of attosecond pulses and signifies important progress in arbitrary optical waveform characterization.

DOI: 10.1103/PhysRevA.101.043416

I. INTRODUCTION

Probing or manipulation of ultrafast electron dynamics on a subfemtosecond ($\leqslant 10^{-15}$ s) or attosecond ($\sim 10^{-18}$ s) timescale necessitates ultrashort laser pulses lasting only a few or near-single optical cycles with controllable waveforms [1–7]. Developments in frequency comb technology combined with pulse-shaping methods have allowed arbitrary electromagnetic waveforms to be synthesized at optical frequencies [8–11]. Knowledge of the temporal structure of these light pulses is a prerequisite for subsequent applications. Traditional characterization techniques, such as frequency-resolved optical gating (FROG), spectral phase interferometry for direct electric field reconstruction (SPIDER) or dispersion scan (d-scan), have been used to measure the spectral or temporal amplitude or phase or dispersion or chirp of short pulses [12–14]. However, the phase-matching problem of nonlinear crystals and the deficiency in determining the absolute phase (carrier-envelope phase, CEP) both limit their applicability. Instead, direct access to the time-domain electric field $\mathbf{E}_L(t)$ requires a fast nonlinear response that is significantly shorter than an optical cycle [15,16].

Advancements in strong-field physics have provided such ultrashort temporal gates. One widely used technique is the attosecond streak camera [17–20]: isolated attosecond XUV pulses generated by higher-order harmonic generation (HHG) processes are used to ionize atoms [21–26]. The ejected photoelectrons are then streaked to different final energies by the test laser field whose waveform is to be measured. The temporal structure of both the test laser and the attosecond XUV pulse can be accurately reconstructed from the streaking photoelectron spectra [27,28]. Two other all-optical characterization methods, petahertz optical oscilloscopy and attosecond spatial interferometry, both utilize the subfemtosecond tunneling-recombination process during HHG generation as the temporal gate to sample the test optical laser field [29,30].

Although these recent characterization techniques yield good performance, their requirement of generation or manipulation of broadband isolated attosecond XUV pulses is still very challenging to meet [31–33]. In this work, we propose a method to extract the waveforms of unknown laser pulses with commonly used strong near-infrared (NIR) tabletop laser light as a pump field to irradiate the atoms. Our proposal utilizes facilities from the strong-field ionization and strong-field photoelectron holography (SFPH) fields [34], and information of the weak test laser pulses is imprinted in the holographic interference fringes of the final photoelectron momentum distribution (PMD).

A strong NIR laser is able to tunnel ionized atoms, and the liberated photoelectron may be driven back and elastically scattered off the parent ion at a later time [35]. Concerning SFPH, strong-field tunneling ionization plays the role of an atomic-level beamsplitter: after tunneling, part of the photoelectron wave packet less impacted by the ionic Coulomb potential forms a reference wave. The other part, termed the signal wave, is steered around and scatters off the atomic core. The hologram stemming from interference of the reference and signal waves at the detector encodes spatiotemporal information about the interaction of the electron-ion system. Recently, the interpretation of SFPH has been improved by the discovery of the glory rescattering effect in strong-field ionization [36].

II. SIMULATION AND DISCUSSION

For theoretical demonstration purposes, a fundamental pump laser field with a wavelength of 800 nm and an intensity of 1.5×10^{14} W/cm^2 is used to ionize hydrogen

*xia_qinzhi@iapcm.ac.cn

†jliu@gscaep.ac.cn

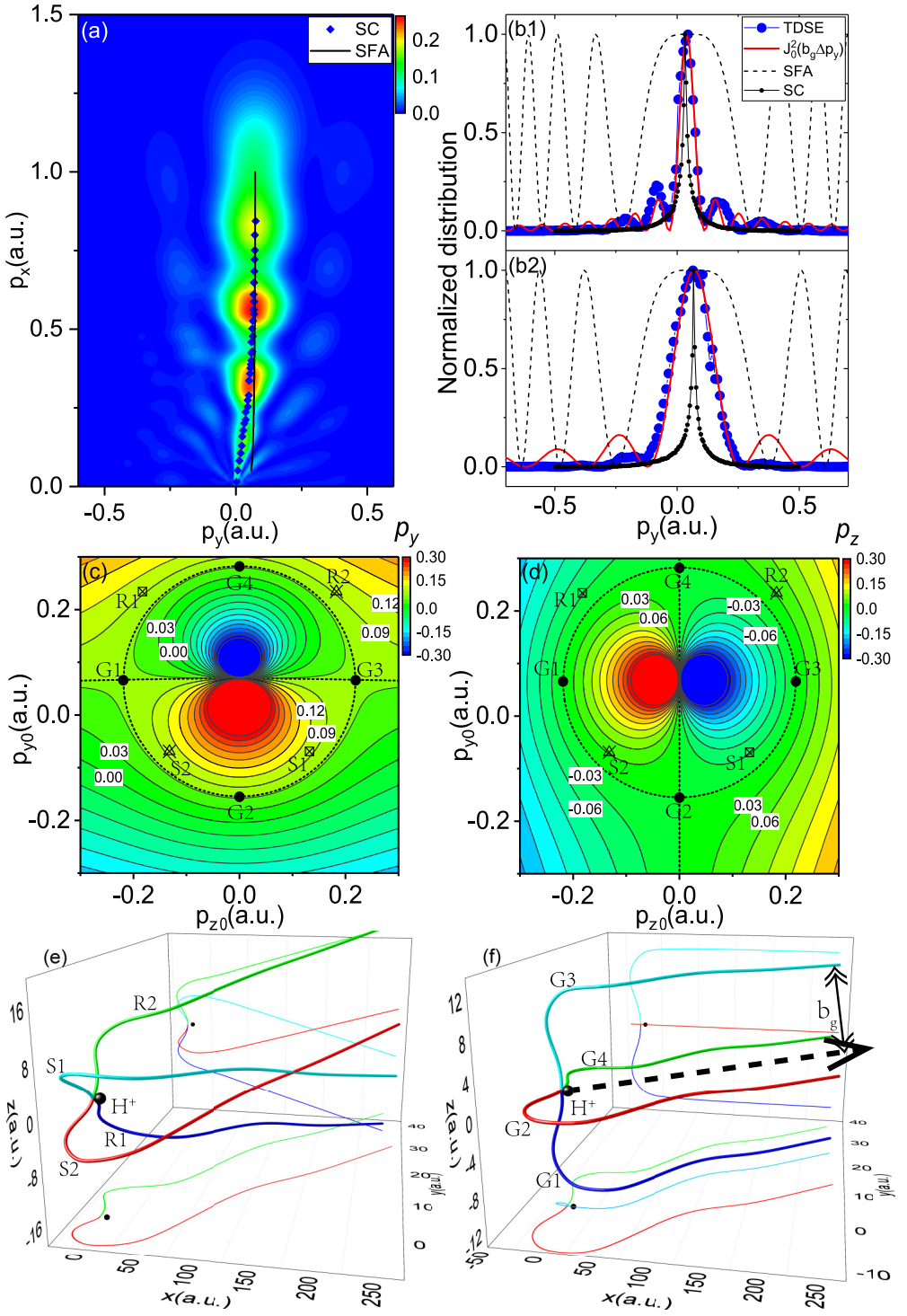

FIG. 1. (a) PMD calculated using the TDSE in the polarization plane ($p_z = 0$), and ionization of H atoms by an OTC laser field. The glory interference maxima (GIM) estimated by the semiclassical method (SC, blue diamonds) and strong-field approximation (SFA, black solid line) are also presented. (b1, b2) Normalized transverse momentum distribution with $p_x = 0.2$ (b1) and 0.6 (b2). Note that the SFA curves have been shifted to match the peak positions calculated by the SC and TDSE. (c, d) Contour plots of the deflection functions with $\eta_0 = 0.3$ and $p_x \approx 0.6$. The circle contour indicates the initial conditions of glory trajectories (GTs), while four typical GTs (G1, G2, G3, and G4) are shown in (f) with XY and XZ projections. (e) Two pairs of signal or reference trajectories with initial conditions from regions (S1, R1) and (S2, R2). See the text for more details.

atoms: $\mathbf{E}_0(t) = \epsilon_0 \cos^2(\frac{\pi t}{T_0}) \cos(\omega_0 t)\hat{\mathbf{x}}$, where $T_0 = 3 \times \frac{2\pi}{\omega_0}$, with the time duration only three optical cycles to eliminate multiple rescattering effects. Figure 1(a) illustrates the PMD in the polarization plane simulated using the time-dependent Schrödinger equation (TDSE) [37] with an orthogonally polarized two-color (OTC) laser field. The test

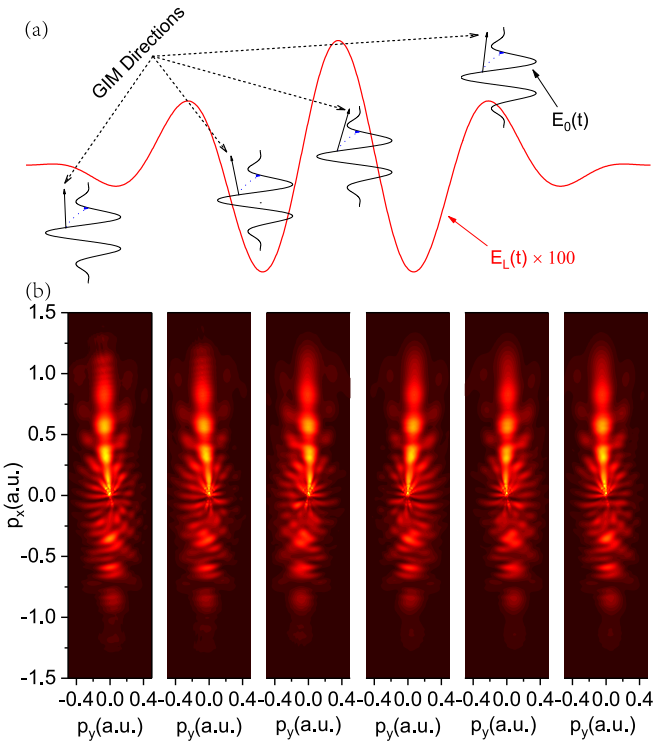

FIG. 2. (a) Illustration of the sampling of a test laser field with the subfemtosecond glory rescattering process. Blue dashed arrows indicate the subcycle excursion of the tunneled electrons. (b) Integrated PMD simulated using the TDSE with time delay $\Delta\tau = \frac{n}{6}$ o.c., where $n = -6, -4, -2, 2, 4, 6$ (left to right). 1 o.c. $= \frac{2\pi}{\omega_0}$.

laser pulse has a wavelength of 1600 nm, an intensity of $2.4 \times 10^{11}\mathrm{W/cm^2}$, and a time duration of four optical cycles: $\mathbf{E}_L(t) = \epsilon_L \cos^2(\frac{\pi t}{T_L})\cos(\omega_L t)\hat{\mathbf{y}}$, with $T_L = 4 \times \frac{2\pi}{\omega_L}$. The spiderlike interference fringes characteristic of SFPH are clearly visible [34]. Unless stated otherwise, atomic units will be used throughout.

Without considering the Coulomb potential, the phase difference responsible for the hologram between the signal and reference photoelectron waves can be derived using strong-field approximation (SFA) or approximations from the path-integral method as follows [34,38,39]:

$$\delta\phi \approx \tfrac{1}{2}(\mathbf{p}_\perp - \mathbf{k}_L)^2\left(t_r - t_0^{ref}\right), \tag{1}$$

in which $\mathbf{p}_\perp$ is the asymptotic photoelectron momentum perpendicular to the fundamental laser polarization, t_r is the rescattering time, and t_0^{ref} is the ionization time of the reference photoelectron wave. The intermediate canonical momentum between tunneling and rescattering is $\mathbf{k}_L = -\frac{1}{t_r - t_0^R}\int_{t_0^R}^{t_r} \mathbf{A}_L(t')dt'$ to ensure that the electron travels back to the ion, while t_0^R is the ionization time of the rescattering wave packet. Generally, for near-forward rescattering with a small transverse momentum $\mathbf{p}_\perp$, the tunneling times for reference and rescattering(signal) quantum paths are approximately the same: $t_0^{\mathrm{ref}} \approx t_0^R$. $\mathbf{A}_L(t) = -\int^t \mathbf{E}_L(t')dt'$ is the vector potential of the weak test laser field.

However, a cos[Re($\delta\phi$)]-like peak structure derived from Eq. (1) for the transverse momentum distribution [black dashed lines in Figs. 1(b1) and 1(b2) for different asymptotic longitudinal momenta $p_x = 0.2, 0.6$] fails to reproduce the TDSE results (blue dotted lines). This problem can be clarified from the semiclassical (SC) perspective of the Feynman path-integral method, which dictates that the dominant contributions come from the regions around the classical trajectories. Figures 1(c) and 1(d) depict the contour plots of the deflection functions $\mathbf{p}_\perp = \mathbf{p}_\perp(\eta_0, \mathbf{p}_{\perp 0})$ obtained by solving Newton's equation of motion after the electron emerges at $\eta_0 = \omega_0 t_0 = \omega_0 \mathrm{Re}(t_0^{\mathrm{ref}}) \approx 0.3$ [40,41]. Due to Coulomb potential influence, the p_{y0}–p_{z0} plane can be divided into four signal or reference regional pairs: (S1, R1), (S2, R2), (S3, R3), and (S4, R4) (with the latter two not shown). For the final photoelectron momentum originating from inside these pairs, only two classical trajectories are found [Fig. 1(e)]; however, infinite classical trajectories stemming from the circle contour dividing the signal and reference regions all contribute to the same asymptotic momentum [Fig. 1(f) depicts four such classical orbits].

This phenomenon is analogous to the (forward) glory effect in quantum scattering theory [42]. The contributions of infinite so-called glory trajectories to the final momentum distribution should be summed up. Referring to Eq. (1), for simplicity, consider the case with only the NIR fundamental pulse; for a small deviation $\Delta p_\perp$ from the forward direction, we have $\Delta[\mathrm{Re}(\delta\phi)] \sim \Delta p_\perp p_{\perp 0}(t_r - t_0) \sim \Delta p_\perp b_g$, where $p_{\perp 0} \neq 0$ is the initial transverse momentum with the Coulomb potential involved. $b_g \sim p_{\perp 0}(t_r - t_0)$ is interpreted as the asymptotic impact factor of GTs [Fig. 1(f)] [36]. Then the transverse momentum distribution in the near-forward direction is $f(p_\perp) \propto |\frac{1}{2\pi}\int_0^{2\pi} e^{i\Delta p_\perp b_g \cos\theta} d\theta|^2 = J_0^2(b_g \Delta p_\perp)$. In an OTC field, this would result in $f(p_\perp) \propto J_0^2(b_g|\mathbf{p}_\perp - \mathbf{p}_L|)$. $\mathbf{p}_L$ is the transverse momenta corresponding to the primary glory interference maxima (GIM) [on the circle contour in Figs. 1(c) and 1(d), $|\mathbf{p}_\perp - \mathbf{p}_L| \equiv 0$]. This result has successfully interpreted the near-forward SFPH interference fringes in PMD [36,39,43].

Using this SC photoelectron trajectory method, b_g can be retrieved by backpropagation for each p_x [36]. The resulting squared-Bessel-like peak structure [red solid lines in Figs. 1(b1) and 1(b2)] agrees very well with the TDSE simulation. A SC trajectory Monte Carlo simulation also reproduces the position of the GIM $\mathbf{p}_L$ [blue diamonds in Fig. 1(a), black dotted lines in Figs. 1(b1) and 1(b2)]. An approximation of this position can be found from Eq. (1) [44]: $\mathbf{p}_L \approx \mathrm{Re}(\mathbf{k}_L)$. This result, shown in Fig. 1(a) (black solid line), describes the TDSE/SC simulations quite well, especially for larger longitudinal photoelectron momentum p_x. The deviation for smaller p_x is due to the Coulomb effects.

III. RETRIEVAL OF VARIOUS OPTICAL WAVEFORMS

Therefore, adding a weak test laser $\mathbf{E}_L(\perp \mathbf{E}_0)$ introduces an extra factor into the phase difference between the reference and signal photoelectron waves [Eq. (1)] or, classically, slightly perturbs the whole bunch of glory rescattering trajectories [Fig. 1(f)]. One of the consequences is a peak shift of the asymptotic transverse momentum distribution, the same as that in nondipole strong-field ionization [41,44–48]. Therefore, we can utilize the subfemtosecond glory rescattering process as a fast temporal gate to sample a test laser pulse

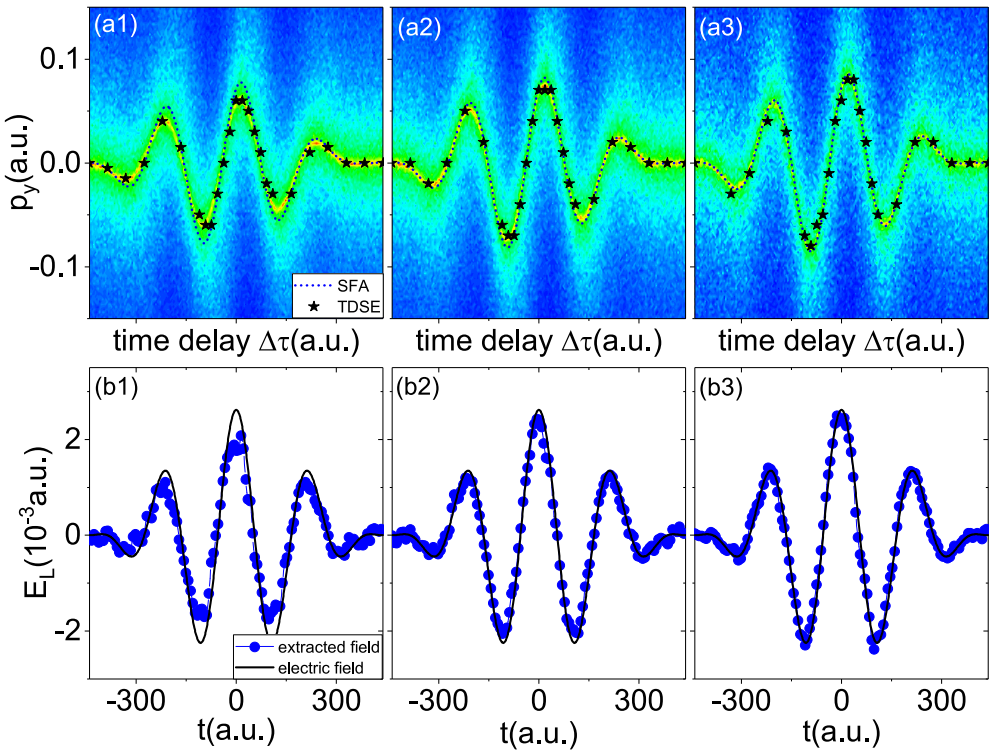

FIG. 3. (a1)–(a3) Streaking spectra of the photoelectron momentum along the test laser polarization direction vs time delay for $p_x = 0.4$ (a1), 0.6 (a2), and 0.8 (a3). The TDSE results (black stars) well fit the SC trajectory Monte Carlo simulation results. Blue short dotted lines are estimated using Eq. (2). (b1)–(b3) Corresponding electric fields (blue dotted lines) extracted from the GIM compared with the actual field (black solid lines).

by varying the time delay between the fundamental and weak light pulses [Fig. 2(a)]:

$$\mathbf{p}_L(\Delta\tau) \approx \mathrm{Re}\left\{-\frac{1}{t_r - t_0^R}\int_{t_0^R+\Delta\tau}^{t_r+\Delta\tau} \mathbf{A}_L(t)dt\right\}. \tag{2}$$

Figure 2(b) illustrates the TDSE simulation of PMDs with different time delays; the GIM oscillates with $\Delta\tau$. If the test light pulse does not contain frequency components (ω) that are larger than about ω_0, we can retrieve the waveform of the test light from the measured GIM as $\mathbf{A}_L(t) \approx -\mathbf{p}_L(t - t_\alpha) + t_\beta^2 \frac{d^2}{dt^2}\mathbf{p}_L(t - t_\alpha)$ for larger longitudinal momentum ($p_x \sim (50\%, 90\%) \times \frac{\epsilon_0}{\omega_0}$) [49]; the second term on the right-hand side is much smaller than the first in the present setup. $t_{\alpha,\beta}$ are small time parameters determined by the fundamental ionizing laser field. Current experiments can measure the smallest transverse momentum amounting to that carried by a few photons, which is on the order of $\delta p_c \sim 10^{-3}$ a.u. [45,48,50]. It is sufficient to resolve the peak positions in our scheme ($\frac{\epsilon_L}{\omega_L} \gg \delta p_c$). In the following demonstrations we have also chosen the upper bound of the difference between two consecutively sampled peak shifts, estimated as $\delta p_\perp \sim \epsilon_L \frac{\sinh \omega_L t_i}{\omega_L t_i}\delta t$, to be slightly larger: $\delta p_\perp \gtrsim \delta p_c$, where $t_i = \mathrm{Im}(t_0^R)$, and δt is the time step associated with changing the time delay between the fundamental and test laser fields.

The streaking photoelectron spectra of the transverse momentum distribution versus time delay are presented in Figs. 3(a1), 3(a2), and 3(a3) for different final longitudinal momenta $p_x = 0.4, 0.6, 0.8$. The same test laser light is used as in Fig. 1. TDSE results (black stars) agree very well with the SC simulation results. The SFA calculation yields a good approximation [blue solid lines in Figs. 3(a1), 3(a2), and 3(a3)]. More precisely, the electric field of the test laser pulse can be directly solved from Eq. (2):

$$\mathbf{E}_L(t) = \frac{1}{i\pi}\int_{-\infty}^{\infty} \frac{\omega\tilde{\mathbf{p}}_L(\omega)}{a(\omega) + a^*(-\omega)} e^{i\omega t} d\omega, \tag{3}$$

where $\tilde{\mathbf{p}}_L(\omega) = \int_{-\infty}^{\infty} \mathbf{p}_L(\Delta\tau)e^{-i\omega\Delta\tau}d\Delta\tau$ is the corresponding Fourier transform, and $a(\omega) = -\int_{t_0^R}^{t_r} e^{i\omega t'}dt'/(t_r - t_0^R)$. The extracted electric field is depicted as blue dotted lines in Figs. 3(b1), 3(b2), and 3(b3). It reproduces the original test laser electric field (black solid lines).

The test optical laser is superimposed on the fundamental pump pulse with perpendicular polarization, and in principle, the waveform of a test laser pulse with complex polarization states can be measured and reconstructed [30]. As an example, the streaking photoelectron spectra in two independent polarization directions are shown in Figs. 4(a) and 4(b) for a light pulse with time-varying ellipticity synthesized by two counterpropagating circularly polarized laser beams: $\mathbf{E}_l = \epsilon_L f_L(t - t_d/2)[\cos(\omega_L t + \frac{\pi}{4})\hat{\mathbf{y}} + \sin(\omega_L t + \frac{\pi}{4})\hat{\mathbf{z}}]$ and $\mathbf{E}_r = \epsilon_L f_L(t + t_d/2)[\cos(\omega_L t + \frac{\pi}{4})\hat{\mathbf{y}} - \sin(\omega_L t + \frac{\pi}{4})\hat{\mathbf{z}}]$.[1]

[1]The carrier frequency is $\omega_L = 0.038$ a.u., corresponding to a wavelength of 1200 nm, with a time duration of $T_L = 4 \times \frac{2\pi}{\omega_L}$, $T_d = T_L/2$. And $\epsilon_L = 0.08 \times \epsilon_0$.

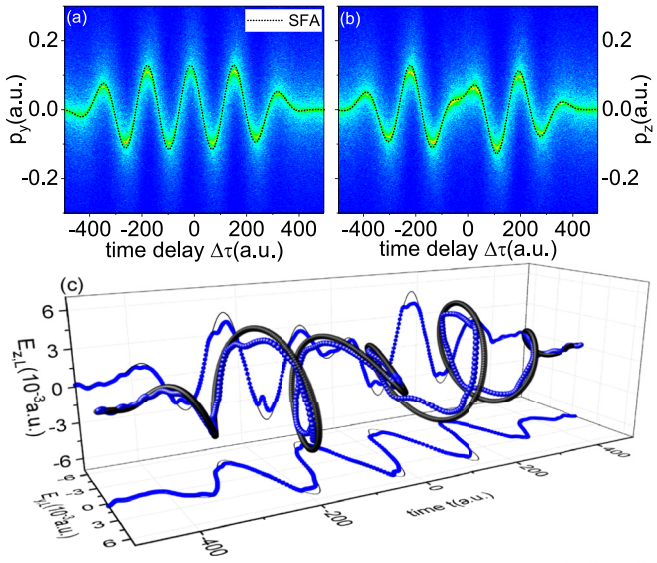

FIG. 4. (a, b) Streaking photoelectron momentum spectra for two independent polarization directions of the synthesized test laser light with time-varying ellipticity ($p_x = 0.8$). (c) 3D representation of the extracted electric field (blue spheres). The result is compared to the synthesized waveform (black spheres); the reconstructed electric fields in the $\hat{\mathbf{y}}$ and $\hat{\mathbf{z}}$ directions (blue dotted lines) are also shown in the projections alongside the respective actual fields (black solid lines).

The same retrieval algorithm is used to simultaneously extract the two electric fields [Fig. 4(c)]. For all of these complex test light conditions, our method yields good results. In the frequency domain, we have the relationship $\tilde{\mathbf{p}}_L(\omega) = r(\omega)\tilde{\mathbf{A}}_L(\omega)$; the frequency response function $r(\omega)$ has approximate magnitude unity until up to about ω_0, so although for demonstration purposes we have mostly used near-monochromatic pulses, this approach is also suitable for retrieval of optical waveforms with broad spectral bandwidths. By decreasing the wavelength of the fundamental ionizing laser field, this method can be used to measure the electromagnetic waveforms in the visible, infrared, and even terahertz regimes.

IV. CONCLUSION

In summary, by leveraging the subfemtosecond Coulomb glory rescattering effect as a fast temporal gate, we can sample arbitrary optical waveforms directly in the time domain with electron spectroscopy and reconstruct the temporal structure of the vectorial optical laser pulses. Compared to easily implementable traditional methods like FROG or electro-optical sampling of terahertz pulses, our approach represents an alternative photoelectron-based method and further improvement of experimental technicalities can be anticipated. Our method completely avoids the use of attosecond XUV optics, and a conventional experimental setup related to strong-field ionization research is sufficient to provide the required data. Our results will facilitate the study of ultrafast electron dynamics in attosecond physics and may open a way to study the properties of the strong-field tunneling wave packet.

ACKNOWLEDGMENTS

J.C. contributed significantly to the time-dependent Schrödinger equation simulations. This work is supported by the National Natural Science Foundation of China (Grants No. 11674034, No. 11822401, No. 11974057, and No. 11447015) and the NSAF (Grant No. U1930402).

APPENDIX A: NUMERICAL SIMULATION WITH TIME-DEPENDENT SCHRöDINGER EQUATION (TDSE)

The three-dimensional TDSE for a hydrogen atom subjected to an orthogonal two-color (OTC) laser field is solved using the generalized pseudospectral split-operator method [51] with single-active-electron approximation. The TDSE in the presence of a strong laser field can be written as

$$i\frac{\partial}{\partial t}\Psi(\mathbf{r},t) = [\hat{H}_0 + \hat{H}_I]\Psi(\mathbf{r},t). \tag{A1}$$

Here, $\hat{H}_0 = \frac{\hat{\mathbf{p}}^2}{2} - \frac{1}{\sqrt{\hat{\mathbf{r}}^2}}$ is the field-free Hamiltonian, and $\hat{H}_I$ is the laser-atom interaction Hamiltonian in length gauge with dipole approximation [52],

$$\hat{H}_I = \mathbf{E}(t)\cdot\hat{\mathbf{r}}, \tag{A2}$$

in which $\mathbf{E}(t) = \mathbf{E}_0(t-\Delta\tau) + \mathbf{E}_L(t)$. The radial grid size is $R_{\max} = 150$ a.u., while the maximum angular momentum quantum number is up to $l_{\max} = 159$, the angular grid number is 180×360, and the propagation time step is $\Delta t = 0.1$ a.u. In order to eliminate the reflection of the electron wave packet from the boundary and obtain the momentum-space wave function, the coordinate space is split into the inner and the outer regions with the critical boundary $R_c = 60$ a.u. (the quiver distance due to the laser fields in our setup is about $\frac{\epsilon}{\omega^2} \sim 20$ a.u. $\ll R_c$), and the electron wave function can be written as [53,54]

$$\Psi(\mathbf{r},t) = \Psi^{\text{in}}(t) + \Psi^{\text{out}}(t). \tag{A3}$$

The inner-region wave function Ψ^{in} is propagated under the full Hamiltonian numerically, while in the outer region, the wave function is projected to momentum space for every 50 time steps $t_{\mathfrak{p}}$:

$$C(\mathbf{p},t_{\mathfrak{p}}) = \langle\Psi^{CV}_{\mathbf{p}}(t_{\mathfrak{p}})|\Psi^{\text{out}}(t_{\mathfrak{p}})\rangle. \tag{A4}$$

Here $\Psi^{CV}_{\mathbf{p}}(t)$ is the Coulomb-Volkov state [55–58]. Then the evolution of $C(\mathbf{p},t_{\mathfrak{p}})$ to the end of the laser field ($t_{\mathfrak{f}}$) is governed by the Volkov propagator $U_V(t_{\mathfrak{f}},t_{\mathfrak{p}}) = \exp(-\frac{i}{2}\int_{t_{\mathfrak{p}}}^{t_{\mathfrak{f}}}[\mathbf{p}+\mathbf{A}(t')]^2]dt')$[53]. Finally, the ionized electron wave function is obtained as

$$\Phi(\mathbf{p}) = \sum_{\mathfrak{p}} U_V(t_{\mathfrak{f}},t_{\mathfrak{p}})C(\mathbf{p},t_{\mathfrak{p}}) + \langle\Psi^{CV}_{\mathbf{p}}(t_{\mathfrak{f}})|\Psi^{\text{in}}(t_{\mathfrak{f}})\rangle. \tag{A5}$$

The last term in the above equation takes into account the ionized electron in the inner-region wave function at the end of the laser pulse.

APPENDIX B: STRONG-FIELD PHOTOELECTRON HOLOGRAPHY AS THE INTERFERENCE OF REFERENCE AND SIGNAL WAVES

Thanks to the pioneering work on strong-field photoelectron holography (SFPH) [34], the interference pattern in the final momentum distribution can be attributed to the interference of an electron wave which reaches the detector directly with little Coulomb disturbance (reference or direct wave) and that which scatters off the parent ion (signal or rescattering wave). The phase difference between the reference and signal waves mostly determines the interference pattern in the momentum distribution:

$$\begin{aligned} P &= |M_s + M_r|^2 \\ &= |M_s|^2 + |M_r|^2 + 2|M_s||M_r|\cos(\Delta S). \end{aligned} \tag{B1}$$

From the derivation by the strong-field approximation (SFA), the phase factors for the reference and signal waves can be written respectively as

$$S_{\text{ref}} = \frac{1}{2}\int_{t_0^{\text{ref}}}^{\infty} d\tau[\mathbf{p} + \mathbf{A}(\tau)]^2 - I_p t_0^{\text{ref}} \tag{B2}$$

and

$$S_{\text{signal}} = \frac{1}{2}\int_{t_r}^{\infty} d\tau[\mathbf{p} + \mathbf{A}(\tau)]^2 + \frac{1}{2}\int_{t_0^R}^{t_r} d\tau[\mathbf{k} + \mathbf{A}(\tau)]^2, -I_p t_0^R \tag{B3}$$

where I_p is the ionization potential of the atom. $\mathbf{k}$ is the intermediate canonical momentum between tunneling and rescattering for the signal wave. $\mathbf{p}$ is the final asymptotic photoelectron momentum.

To solve for the various tunneling and rescattering times $(t_0^{\text{ref}}, t_0^R, t_r)$, the saddle-point approximation will be used for the reference [Eq. (B2)] and signal [Eq. (B3)] waves, respectively:

$$\frac{1}{2}\left[\mathbf{p} + \mathbf{A}\left(t_0^{\text{ref}}\right)\right]^2 + I_p = 0, \tag{B4}$$

and

$$\begin{aligned} &\frac{1}{2}\left(\mathbf{k} + \mathbf{A}\left(t_0^R\right)\right)^2 + I_p = 0 \\ &(\mathbf{k} + \mathbf{A}(t_r))^2 = [\mathbf{p} + \mathbf{A}(t_r)]^2 \\ &\int_{t_0^R}^{t_r} [\mathbf{k} + \mathbf{A}(\tau)]d\tau = 0. \end{aligned} \tag{B5}$$

The phase difference can be derived as

$$\begin{aligned} \Delta S = &\frac{1}{2}\int_{t_0^{\text{ref}}}^{t_r} d\tau[\mathbf{p} + \mathbf{A}(\tau)]^2 - \frac{1}{2}\int_{t_0^R}^{t_r} d\tau[\mathbf{k} + \mathbf{A}(\tau)]^2 \\ &+ I_p\left(t_0^R - t_0^{\text{ref}}\right). \end{aligned} \tag{B6}$$

The test weak laser field has negligible influence on the derivation of the tunneling and rescattering time $t_0^{\text{ref}}, t_0^R, t_r$. Moreover, for forward scattering with small transverse momentum $\mathbf{p}_\perp$, analysis shows that [59] $t_0^R \approx t_0^{\text{ref}}$, $k_x \approx p_x$, and $\text{Im}(t_r) \approx 0$, with these simplifications, and the phase difference in Eq. (B6) for near-forward scattering can be derived as

$$\begin{aligned} \Delta S \approx &\int_{t_0^{\text{ref}}}^{t_0^R}\left[\frac{1}{2}(p_x + A_x(\tau)\right]^2 + I_p)d\tau \\ &+ \frac{1}{2}\int_{t_0^{\text{ref}}}^{t_r}([\mathbf{p}_\perp + \mathbf{A}_\perp(\tau)]^2 \\ &- [\mathbf{k}_\perp + \mathbf{A}_\perp(\tau)]^2)d\tau \\ = &\frac{1}{2}\int_{t_0^{\text{ref}}}^{t_r}[\mathbf{p}_\perp^2 - \mathbf{k}_\perp^2 + 2\mathbf{p}_\perp \cdot \mathbf{A}_\perp(\tau) - 2\mathbf{k}_\perp \cdot \mathbf{A}_\perp(\tau)]d\tau \\ = &\frac{1}{2}(\mathbf{p}_\perp^2 - \mathbf{k}_\perp^2)\left(t_r - t_0^{\text{ref}}\right) + (\mathbf{p}_\perp - \mathbf{k}_\perp)\cdot\int_{t_0^{\text{ref}}}^{t_r}\mathbf{A}_\perp(\tau)d\tau \\ = &\frac{1}{2}(\mathbf{p}_\perp^2 - \mathbf{k}_\perp^2)\left(t_r - t_0^{\text{ref}}\right) + (\mathbf{p}_\perp - \mathbf{k}_\perp)\cdot(-\mathbf{k}_\perp)\left(t_r - t_0^{\text{ref}}\right) \\ = &\frac{1}{2}(\mathbf{p}_\perp - \mathbf{k}_\perp)^2\left(t_r - t_0^{\text{ref}}\right) \\ = &\frac{1}{2}((p_y - k_y)^2 + (p_z - k_z)^2)\left(t_r - t_0^{\text{ref}}\right), \end{aligned} \tag{B7}$$

in which

$$k_{y(z)} = -\frac{1}{t_r - t_0^R}\int_{t_0^R}^{t_r} A_{y(z)}(t')dt'. \tag{B8}$$

In the above derivation, we have used the relationship Eq. (B5).

To retrieve the test laser waveform from the streaked photoelectron momentum distribution, experimentally extracting the peak shift of the transverse momentum distribution $f(p_\perp)$ is needed. Denoting this peak shift which corresponds to the GIM for every time delay as $\mathbf{p}_L(\Delta\tau)$, then we have the approximation from Eq. (B8):

$$\begin{aligned} \mathbf{p}_L(\Delta\tau) &\approx \text{Re}\left\{-\frac{1}{t_r - t_0^R}\int_{t_0^R + \Delta\tau}^{t_r + \Delta\tau}\mathbf{A}_L(t)dt\right\} \\ &= \text{Re}\left\{-\frac{1}{t_r - t_0^R}\int_{t_0^R}^{t_r}\mathbf{A}_L(t + \Delta\tau)dt\right\}. \end{aligned} \tag{B9}$$

Taking the Fourier transform with a variable $\Delta\tau$ of both sides, we have

$$\tilde{\mathbf{p}}_L(\omega) = \tilde{\mathbf{A}}_L(\omega)\frac{a(\omega) + a^*(-\omega)}{2}. \tag{B10}$$

$\tilde{\mathbf{A}}_L(\omega) = \int_{-\infty}^{\infty}\mathbf{A}_L(t)e^{-i\omega t}dt$, $\tilde{\mathbf{p}}_L(\omega) = \int_{-\infty}^{\infty}\mathbf{p}_L(\Delta\tau)e^{-i\omega\Delta\tau}d\Delta\tau$ are the corresponding Fourier transforms, $a(\omega) = -\int_{t_0^R}^{t_r} e^{i\omega t'}dt'/(t_r - t_0^R)$. We can define the frequency response function (FRF) of the measurement process as $r(\omega) = \frac{a(\omega) + a^*(-\omega)}{2}$, which can be interpreted as the Fourier transform of the nominal finite impulse response (FIR): $G(t) = \text{Re}\{-\frac{1}{t_r - t_0^R}\int_{t_0^R}^{t_r}\delta(t' + t)dt'\}$ such that $\mathbf{p}_L(\Delta\tau) = (G * \mathbf{A}_L)(\Delta\tau)$. The amplitude and phase of

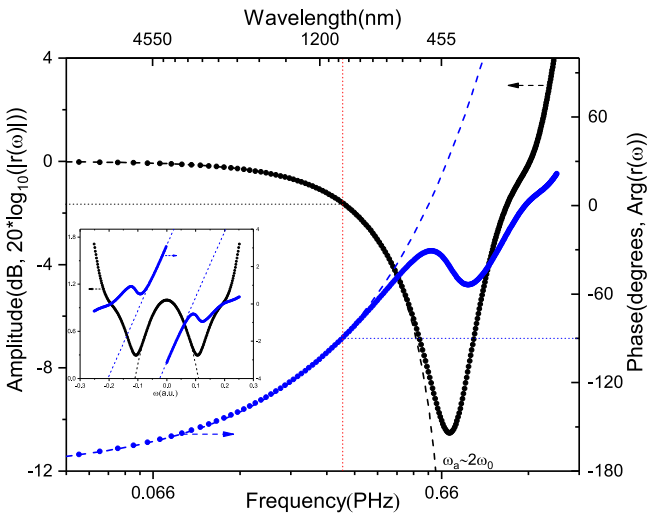

FIG. 5. The amplitude (black dots) and the phase (blue dots) of the frequency response function (FRF). Black and blue dashed lines represent the approximate FRF: $r(\omega) \approx (1 - t_\beta^2 \omega^2) e^{i(\mp\pi + t_\alpha \omega)}$. Inset: with linear scale.

the FRF are plotted in Fig. 5. We can clearly see that no frequency components contained in the test pulse $\mathbf{A}_L(t)$ are significantly suppressed ($|r(\omega)| \geqslant 0.3$, for when $p_x = 0.8$ with the current fundamental ionizing field), so there is no strict restriction on the frequency bandwidth of the test pulse from this perspective. Actually, we do not intend our method to measure electromagnetic waves with very short wavelengths. Other restrictions will be simply discussed below.

Because we use the fast Fourier transform (FFT) algorithm in the retrieval processes, the time step δt associated with changing the delay $\Delta\tau$ should not be chosen arbitrarily. Since $\mathbf{A}_L(t) = \frac{1}{2\pi}\int_{-\infty}^{\infty} r^{-1}(\omega)\tilde{\mathbf{p}}_L(\omega)e^{i\omega t}d\omega$, $r^{-1}(\omega)$ decreases exponentially with increasing ω. We define ω_c as the critical frequency when $r^{-1}(\omega_c)$ is sufficiently small. To ensure that no relevant frequency components are filtered out in the retrieval process, a requirement of δt therefore is

$$\omega_{\text{Nyquist}} = \frac{2\pi}{2\delta t} \geqslant \omega_c. \tag{B11}$$

In our numerical demonstrations with the proposed test laser fields, a time step of about $\delta t \sim 2$ a.u. (48.4 attoseconds) is used; with this time step, $|r^{-1}(\omega_{\text{Nyquist}})| \sim 10^{-10}$. Recent experiments can create a delay step down to 26 attoseconds [60]. With this δt, the Nyquist frequency ω_{Nyquist} corresponds to a wavelength of about 29 nm, which is in the extreme ultraviolet region. This high-frequency component (if with substantial intensity) will strongly distort the tunneling ionization process, rendering our method invalid. δt can be increased in realistic experiments.

Aside from the restriction on the time step δt, the smallest transverse momentum increment $\delta p_\perp$ that can be distinguished by two consecutive measurement steps is also restricted. A rough estimation can be obtained from Eq. (B9), assuming $E_L(t) \approx \epsilon_L \cos\omega_L t$, $t_r - t_0 \ll \frac{2\pi}{\omega_L}[t_0 = \text{Re}(t_0^R)]$:

$$\begin{aligned}\delta p_\perp &= \left|\text{Re}\left\{\frac{1}{t_r - t_0^R}\int_{t_0^R}^{t_r} \mathbf{E}_L(t+\Delta\tau)dt\right\}\right|\delta t \\ &\lesssim \epsilon_L \frac{\sinh\omega_L t_i}{\omega_L t_i}\delta t,\end{aligned} \tag{B12}$$

where $t_i = \text{Im}(t_0^R)$. In the recent study on photon momentum partition and nondipole effects in strong-field ionization [45,48,50], experimentalists are able to resolve the photoelectron transverse momenta amounting to a few photons, on the order of $\delta p_c \sim 10^{-3}$ a.u. With δt used in our simulation, the upper bounds of $\delta p_\perp$ with our test light pulses (Figs. 3 and 4) are about 0.005 and 0.01 a.u. Test laser pulses with larger intensities can be used in experiments [38,49,59]. One may need to resort to statistical spectral analysis for a more detailed estimation.

The electric field of the test laser field can directly be expressed as

$$\mathbf{E}_L(t) = \frac{1}{i\pi}\int_{-\infty}^{\infty} \frac{\omega\tilde{\mathbf{p}}_L(\omega)}{a(\omega) + a^*(-\omega)} e^{i\omega t}d\omega. \tag{B13}$$

APPENDIX C: SEMICLASSICAL TRAJECTORY MONTE CARLO SIMULATION

In our SC model [61], the bounded electron tunnels through the potential barrier formed by the Coulomb potential of the atomic core and the instantaneous laser electric field. The photoelectron (released at the tunneling exit r_0 from the ion) has a Gaussian transverse (with respect to the direction of instantaneous electric field) velocity distribution: $f(v_\perp) = \exp[-\kappa v_\perp^2/|\epsilon(t_0)|]$, $\kappa = \sqrt{2I_p}$, and $\epsilon(t)$ is the instantaneous laser electric field strength [62]. Subsequently, the electron moves in a combined laser electromagnetic field and Coulomb potential governed by Newton's equations of motion: $\frac{d\mathbf{p}}{dt} = -[\mathbf{E}_0(t-\Delta\tau) + \mathbf{E}_L(t)] - \frac{\mathbf{r}}{r^3}$. A large ensemble of electron trajectories on the order of 10^6 is simulated for analysis.

Figure 6 illustrates the integrated two-dimensional PMD: TDSE and SC trajectory Monte Carlo simulations for (a) and (b), respectively. The laser parameters are the same as in Fig. 1. This SC simulation grasps the main feature of the final photoelectron momentum distribution, especially accurately revealing the GIM.

According to the Coulomb glory rescattering theory [36], the transverse momentum distribution in the near-forward direction for a fixed p_x would behave as

$$f(p_\perp) \sim J_0^2[b_g\sqrt{(p_y - p_{y,L})^2 + (p_z - p_{z,L})^2}]. \tag{C1}$$

The GIM in two independent directions (y and z) can be extracted from the final 3D momentum distribution simultaneously, without interfering from the other direction.

Using a shooting method with a fixed final longitudinal momentum p_x, we can reversely extract the initial conditions for the glory trajectories, thus getting the value of the asymptotic impact factor b_g for every p_x. See Fig. 7. A pure SC trajectory Monte Carlo simulation would yield a logarithmiclike peak structure for the transverse momentum distribution [black dotted lines in Figs. 1(b1) and (b2)]; this

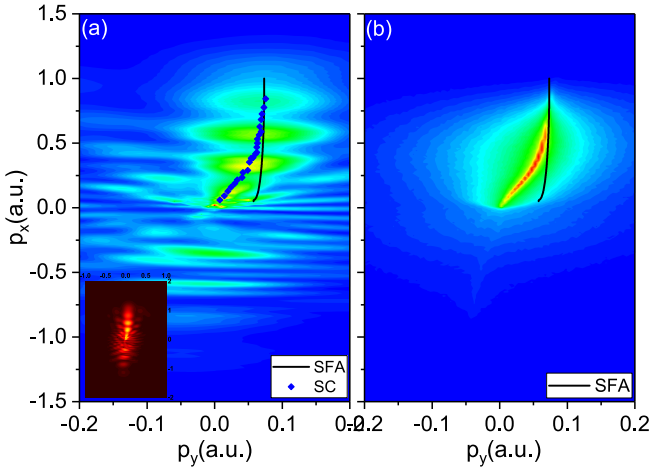

FIG. 6. Integrated photoelectron momentum distribution (PMD) in the polarization direction, ionization of H atom by an OTC laser field with time delay $\Delta\tau = 0$. TDSE and SC Monte Carlo simulations for (a) and (b), respectively. Inset (a): Holographic interference pattern by TDSE simulation. Blue diamonds in panel (a) are the peak shift calculated by SC in panel (b).

results from the mathematical saddle points in the classical deflection function [G1, G3 in Fig. 1(c) are two saddle points of $p_y = p_y(\mathbf{p}_{\perp 0})|_{\eta_0=0.3}$] [63]. Therefore, if the saddle points or, equivalently, the circle contour corresponding to the GTs are not in the regime of significance of the initial transverse momentum distribution, the Coulomb glory rescattering effect would be suppressed. Back to the case discussed in our research, this would roughly require that the electron drift due to the weak test field should not be too large; a very rough estimation would be

$$\frac{\epsilon_L}{\omega_L} \lesssim \sqrt{\frac{\epsilon_0}{\kappa}}. \tag{C2}$$

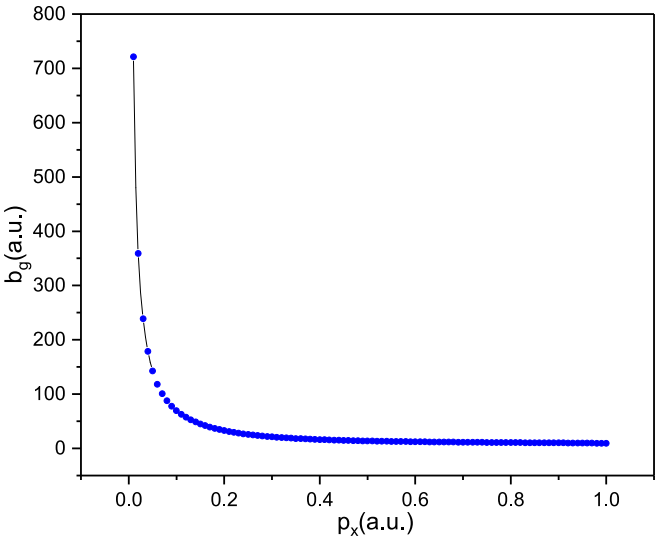

FIG. 7. Extracted asymptotic impact factor of the glory trajectories for different longitudinal momentum p_x.

The same criterion for an elliptically polarized strong laser field has already been found [64]. Moreover, in nondipole strong-field ionization, the transverse momentum drift due to the radiation pressure scales as U_p/c, where $U_p = \frac{\epsilon_0^2}{4\omega_0^2}$ is the ponderomotive potential and c is the speed of light in vacuum. Since the same Coulomb glory rescattering effect causes the counterintuitive peak shift of the transverse momentum distribution in laser propagation direction [44,45], a similar criterion $\frac{U_p}{c} \lesssim \sqrt{\frac{\epsilon_0}{\kappa}}$ holds [65]. Like in the discussion about nondipole ionization, Eq. (C2) is not a strict limitation; the primary requirement is that the intensity of the test laser fields should not be too large to render recollision ineffective.

The momentum drift due to a true electric field will typically be much larger than that due to the radiation pressure $\frac{\epsilon_L}{\omega_L} \gg \frac{U_p}{c}$, so the peak position of transverse momentum distribution may be easier to measure in experiments for our method. With the laser parameters and time step chosen in our simulations, U_p/c is on the same order of $\delta p_\perp$. Fortunately for a particular p_x, the peak shift due to the radiation pressure of the fundamental laser field is a fixed value [48]; therefore if the test laser field is superposed with its polarization parallel to the propagation direction of the fundamental laser field, then a constant value due to the radiation pressure should be subtracted from the measured peak shift of the transverse momentum distribution.

By further inspecting the FRF (Fig. 5), the frequency components near a particular $\omega_a \approx 0.11$ a.u. (corresponding to about 400 nm) are mostly attenuated. Analyses of the FRF with various intensities and frequencies of the fundamental fields indicate that $\omega_a \approx \frac{2\pi}{t_r - t_0} \sim 2\omega_0$. Therefore for our scheme to encompass shorter wavelengths, we can decrease the wavelength of the fundamental laser field. Generally we intend our method to measure the waveforms in the visible, infrared, or even terahertz regimes, with relatively longer wavelengths. From Fig. 5, we also conclude that if the test light pulses only contain components with wavelengths longer than about $\lambda_0 = 800$ nm, the FRF can be expressed as

$$r(\omega) \approx \left(1 - t_\beta^2 \omega^2\right) e^{i(\mp\pi + t_\alpha \omega)}. \tag{C3}$$

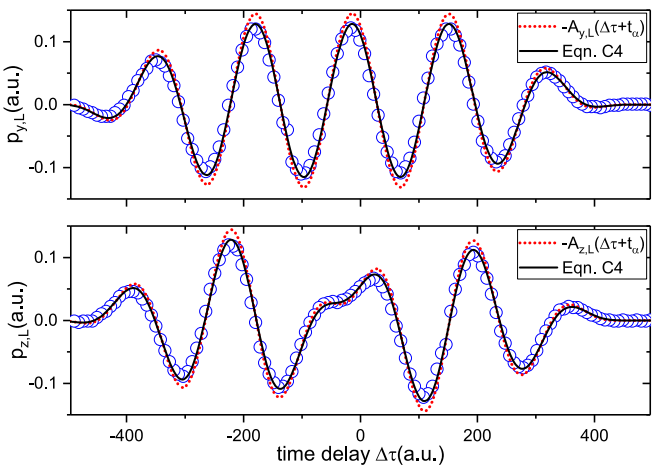

FIG. 8. Blue open circles are the peak shifts extracted from Figs. 4(a) and 4(b).

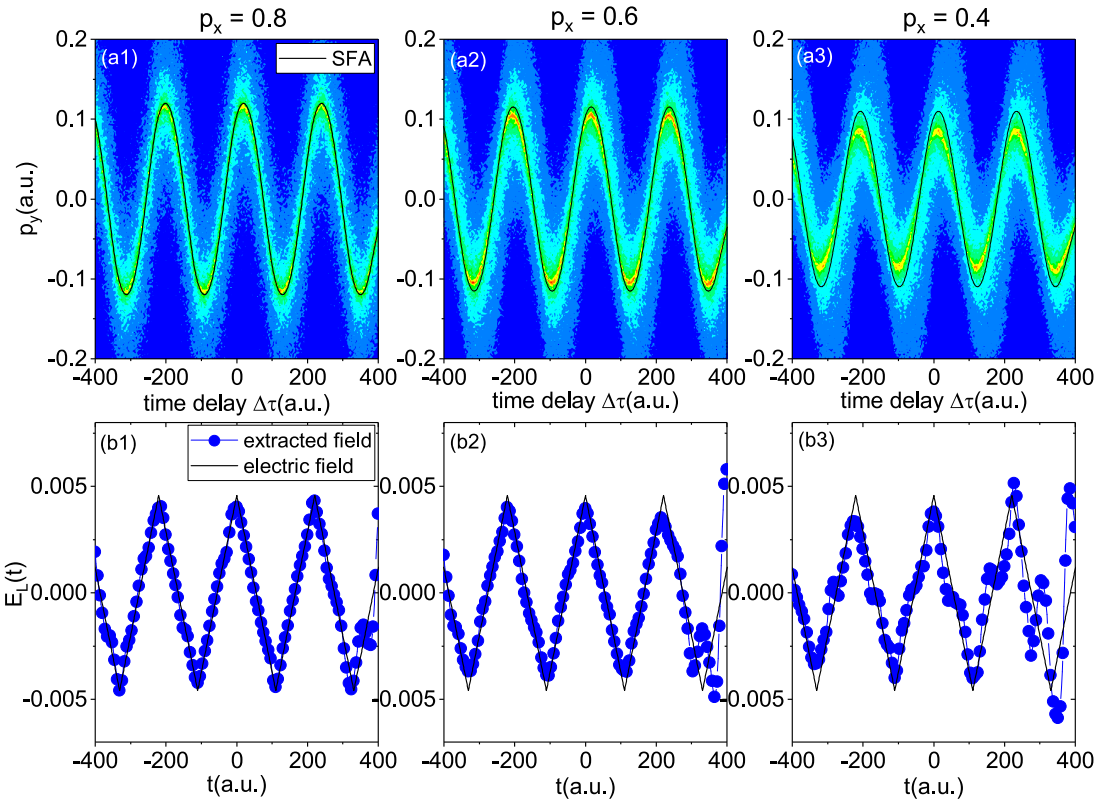

FIG. 9. (a1)–(a3) Streaked photoelectron transverse momentum vs time delay for a triangle test light pulse. The reconstructed electric field is shown in panels (b1)–(b3).

$t_{\alpha,\beta} = t_{\alpha,\beta}(t_0^R, t_r)$ are small time parameters that are determined by the fundamental ionizing laser field (for larger p_x when the Coulomb influence is small) and decrease with increasing ω_0. Further analysis of the FRF shows that $t_\alpha \approx \frac{t_r+t_0}{2}$, $t_\beta \approx \frac{t_r-t_0}{2\sqrt{6}}$ for $\omega \ll \omega_0$. (Note the absence of the imaginary part of the tunneling time; this is another reason why a SC trajectory-based method can yield very good results with longer wavelengths of the test laser fields.) In the current setup, $t_\alpha \approx 35$ a.u., $t_\beta \approx 9$ a.u. Then we have the simple relationship

$$\mathbf{p}_L(\Delta\tau) \approx -\mathbf{A}_L(\Delta\tau + t_\alpha) + t_\beta^2 \frac{d\mathbf{E}_L}{d\Delta\tau}(\Delta\tau + t_\alpha), \quad \text{(C4)}$$

where the second term on the right-hand side is much smaller than the first term in the current setup. Numerical simulations confirm this relationship (e.g., Fig. 8). If we *naively* decrease the wavelength of the fundamental ionizing field indefinitely, the same result as that in the attosecond streak camera will be achieved. Of course, this is not possible for our scheme.

The reason is that since the fundamental laser field $\mathbf{E}_0$ is used to initiate the strong-field tunneling ionization process, its intensity and wavelength should be adjusted to fall into the tunneling ionization regime. A rough requirement would be that the Keldysh parameter should be small [66]: $\gamma = \sqrt{\frac{I_p}{2U_p}} \lesssim 1$, $U_p = \frac{\epsilon_0^2}{4\omega_0^2}$ is the ponderomotive potential. In the current setup, $\gamma = 0.87$.

We have used a fundamental ionizing laser field with near-single-cycle duration to avoid the multiple rescattering effect [67]. While a laser field with more optical cycles can be used in experiments, to suppress the multiple rescattering effects, optical gating or double optical gating can be used to restrict the recollision process to within one optical cycle [68,69]. Calculations with different combinations of the intensities and carrier frequencies of the fundamental ionizing laser fields

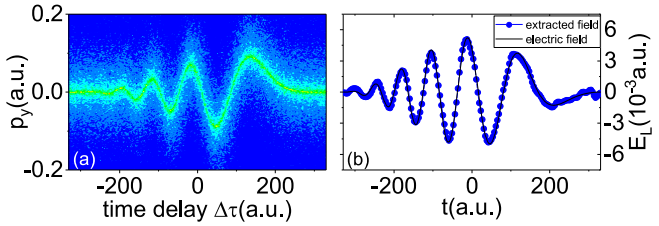

FIG. 10. (a) Streaking spectra for an octave-spanning linearly chirped light pulse ($p_x = 0.8$). (b) The retrieved electric field (blue dotted line).

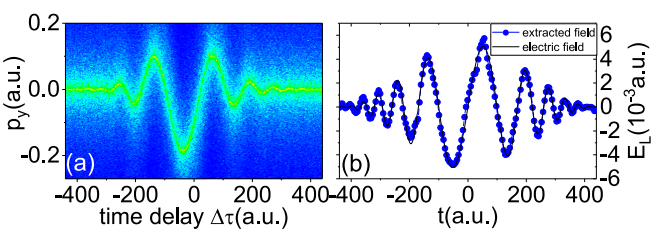

FIG. 11. (a) Streaking spectra for a quadratically chirped light pulse ($p_x = 0.8$). (b) The retrieved electric field (blue dotted line).

indicate that Eq. (C3) is a very good approximation for the FRF $r(\omega)$ when $\omega \lesssim \omega_0$. Of course, if the test laser fields contain significant frequency components that are larger than ω_0, one can still resort to the exact equation Eq. (B13). A choice of the ionizing target with a smaller I_p may by advantageous. In experiments, rare gas atoms like krypton or xenon may be used. Some of these restrictions [Eq. (B11), Eq. (B12), and Eqn. (C2)] may be relaxed a little due to a seemingly redundancy of data, which will be discussed briefly below.

APPENDIX D: DEMONSTRATION OF THE UTILITY OF OUR THEORY WITH MORE WAVEFORMS OF THE TEST LASER FIELDS

Figure 9 depicts the calculated results with a triangle wave. The streaking traces are shown in panels (a1), (a2), and (a3) for different final longitudinal momenta. In panels (b1), (b2), and (b3), the extracted waveform by Eq. (B13) is also illustrated.

In Figs. 10(a) and 10(b), the streaking photoelectron transverse momentum spectra and extracted waveform are depicted for an octave-spanning linearly chirped pulse: $E_L(t) = \epsilon_L f_L(t)\cos(\omega_L t - \frac{\omega_L^2}{12\pi}t^2 + \psi)$, the carrier frequency is $\omega_L = 0.057$ a.u., and the time duration is $T_L = 6 \times \frac{2\pi}{\omega_L}$. ψ is chosen so that $\int E_L(t)dt = 0$. And $\epsilon_L = 0.08 \times \epsilon_0$.

In Figs. 11(a) and 11(b), the streaking photoelectron transverse momentum spectra and extracted waveform are depicted for an quadratically chirped pulse: $E_L(t) = \epsilon_L f_L(t)\sin(\omega_L t + \frac{\omega_L^3}{8\pi^2}t^3)$, the carrier frequency is $\omega_L = 0.028$ a.u., and the time duration is $T_L = 4 \times \frac{2\pi}{\omega_L}$. Also $\epsilon_L = 0.08 \times \epsilon_0$.

APPENDIX E: DISCUSSION OF THE POSSIBILITY OF A NEW STREAK CAMERA SCHEME IN THE ATTOSECOND AND SUBFEMTOSECOND REGIME

In principle, our method is analogous to the attosecond angular streaking (attoclock) technique [70]. While in attoclock, the tunneling photoelectron wave packet (TPW) released by

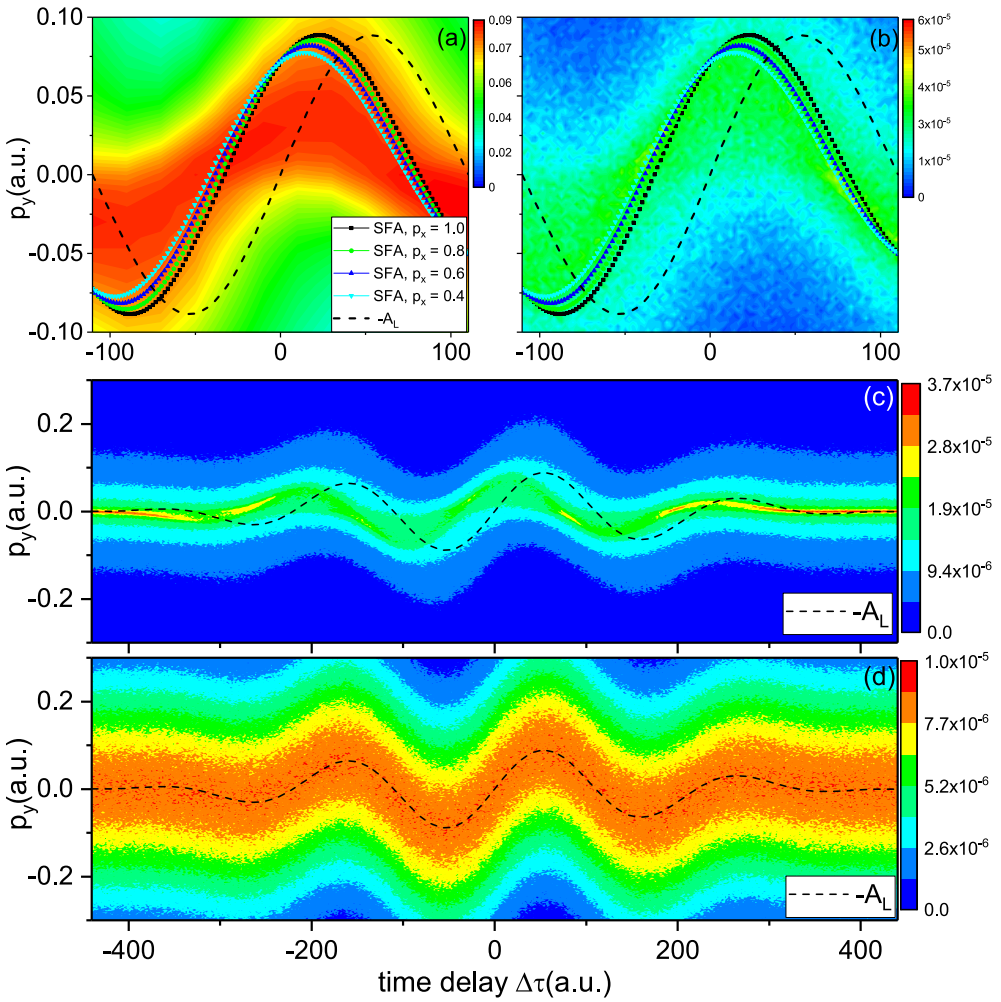

FIG. 12. Integrated streaking asymptotic momentum p_y spectra vs time delay between the pump (central wavelength 800 nm, peak intensity 1.5×10^{14} W/cm^2, time duration three optical cycles) and probe (central wavelength 1600 nm, peak intensity 2.4×10^{11} W/cm^2, time duration four optical cycles) lights. (a) TDSE calculation. (b, c) SC trajectory Monte Carlo simulation results. (d) Similar to (c) but the motion of photoelectrons after tunneling is solved without ionic Coulomb force. In panels (a, b), dotted lines are calculated by SFA with fixed longitudinal momenta p_x.

a strong near-circularly-polarized laser field is streaked to different angles by the same field, yielding a one-to-one mapping between the tunneling time and the final direction of the asymptotic electron momentum. In our scheme, the TPW is released by a strong linearly-polarized laser field, and careful tailoring of the waveform of this pump pulse may lead to a more confined TPW in the time domain [10]. Unfortunately, the glory trajectories released at different tunneling times all contribute to the same direction (parallel to the fundamental laser polarization). Introducing a perpendicularly polarized weak probe field lifts this degeneracy, yielding the one-to-one correspondence between the tunneling time and the direction of infinite glory trajectories [Fig. 1(a), for different p_x (different tunneling time), the glory interference maximum is different]: $t_0 \mapsto \mathbf{p}_L$.

Moreover, our scheme has an extra control knob compared to the attoclock (in which the strong near-circularly-polarized laser field acts both as the pump and the probe): the time delay between the fundamental and test laser pulses can be varied. This indicates that our method also bears some similarities to the attosecond streak camera; in both cases, the photoelectron transverse momentum and energy distribution for every time delay is a mapped replica of the initial photoelectron transients [71]. In Figs. 12(a), 12(b) and 12(c), the integrated streaking transverse momentum spectra versus time delay are demonstrated (with the longitudinal momentum p_x integrated out), the streaking traces are obviously more "broadband"(along the p_y axis). The width is more a measure of the TPW in the time domain rather than a measure of the spread of the initial transverse momentum distribution [Fig. 12(d)] [72].

This seeming redundancy of data may lead to much more robust retrieval schemes. In an attosecond streak camera, this is reflected in the fact that with a time-delayed streaking spectrogram, both the temporal structures of the attosecond XUV and near-infrared light pulses can be retrieved double-blindly with accuracy, and the algorithm is very robust against noises [31]. Our scheme may finally evolve to a similar status. However, before that, a feasible theory that can nicely account for the Coulomb effects should be developed [Eq. (B9) fails especially for small p_x due to Coulomb potential influence.] Although this theory is still lacking, our present work represents a first step toward a new streaking scheme in the attosecond and subfemtosecond regime, which may be used to probe the tunneling photoelectron transients or to time the recollision dynamics [49,73], since rescattering is inherent in the present scheme.

[1] E. Goulielmakis, V. S. Yakovlev, A. L. Cavalieri, M. Uiberacker, V. Pervak, A. Apolonski, R. Kienberger, U. Kleineberg, and F. Krausz, Science **317**, 769 (2007).

[2] M. Kremer, B. Fischer, B. Feuerstein, V. L. B. de Jesus, V. Sharma, C. Hofrichter, A. Rudenko, U. Thumm, C. D. Schröter, R. Moshammer, and J. Ullrich, Phys. Rev. Lett. **103**, 213003 (2009).

[3] A. Schiffrin, T. Paasch-Colberg, N. Karpowicz, V. Apalkov, D. Gerster, S. Mühlbrandt, M. Korbman, J. Reichert, M. Schultze, S. Holzner, J. V. Barth, R. Kienberger, R. Ernstorfer, V. S. Yakovlev, M. I. Stockman, and F. Krausz, Nature (London) **493**, 70 (2012).

[4] N. Ishii, K. Kaneshima, K. Kitano, T. Kanai, S. Watanabe, and J. Itatani, Nat. Commun. **5**, 3331 (2014).

[5] M. Garg, M. Zhan, T. T. Luu, H. Lakhotia, T. Klostermann, A. Guggenmos, and E. Goulielmakis, Nature (London) **538**, 359 (2016).

[6] A. Sommer, E. M. Bothschafter, S. A. Sato, C. Jakubeit, T. Latka, O. Razskazovskaya, H. Fattahi, M. Jobst, W. Schweinberger, V. Shirvanyan, V. S. Yakovlev, R. Kienberger, K. Yabana, N. Karpowicz, M. Schultze, and F. Krausz, Nature (London) **534**, 86 (2016).

[7] S. Rozen, A. Comby, E. Bloch, S. Beauvarlet, D. Descamps, B. Fabre, S. Petit, V. Blanchet, B. Pons, N. Dudovich, and Y. Mairesse, Phys. Rev. X **9**, 031004 (2019).

[8] S. T. Cundiff and A. M. Weiner, Nat. Photonics **4**, 760 (2010).

[9] H.-S. Chan, Z.-M. Hsieh, W.-H. Liang, A. H. Kung, C.-K. Lee, C.-J. Lai, R.-P. Pan, and L.-H. Peng, Science **331**, 1165 (2011).

[10] A. Wirth, M. T. Hassan, I. Grguraš, J. Gagnon, A. Moulet, T. T. Luu, S. Pabst, R. Santra, Z. A. Alahmed, A. M. Azzeer, V. S. Yakovlev, V. Pervak, F. Krausz, and E. Goulielmakis, Science **334**, 195 (2011).

[11] A. Schliesser, N. Picqué, and T. W. Hänsch, Nat. Photonics **6**, 440 (2012).

[12] R. Trebino, K. W. DeLong, D. N. Fittinghoff, J. N. Sweetser, M. A. Krumbügel, B. A. Richman, and D. J. Kane, Rev. Sci. Instrum. **68**, 3277 (1997).

[13] C. Iaconis and I. A. Walmsley, Opt. Lett. **23**, 792 (1998).

[14] M. Miranda, C. L. Arnold, T. Fordell, F. Silva, B. Alonso, R. Weigand, A. L'Huillier, and H. Crespo, Opt. Express **20**, 18732 (2012).

[15] A. S. Wyatt, T. Witting, A. Schiavi, D. Fabris, P. Matia-Hernando, I. A. Walmsley, J. P. Marangos, and J. W. G. Tisch, Optica **3**, 303 (2016).

[16] S. B. Park, K. Kim, W. Cho, S. I. Hwang, I. Ivanov, C. H. Nam, and K. T. Kim, Optica **5**, 402 (2018).

[17] G. Sansone, E. Benedetti, F. Calegari, C. Vozzi, L. Avaldi, R. Flammini, L. Poletto, P. Villoresi, C. Altucci, R. Velotta, S. Stagira, S. De Silvestri, and M. Nisoli, Science **314**, 443 (2006).

[18] E. Goulielmakis, M. Uiberacker, R. Kienberger, A. Baltuska, V. Yakovlev, A. Scrinzi, T. Westerwalbesloh, U. Kleineberg, U. Heinzmann, M. Drescher, and F. Krausz, Science **305**, 1267 (2004).

[19] J. Itatani, F. Quéré, G. L. Yudin, M. Y. Ivanov, F. Krausz, and P. B. Corkum, Phys. Rev. Lett. **88**, 173903 (2002).

[20] R. Boge, S. Heuser, M. Sabbar, M. Lucchini, L. Gallmann, C. Cirelli, and U. Keller, Opt. Express **22**, 26967 (2014).

[21] M. Lewenstein, P. Balcou, M. Y. Ivanov, A. L'Huillier, and P. B. Corkum, Phys. Rev. A **49**, 2117 (1994).

[22] A. Baltuska, T. Udem, M. Uiberacker, M. Hentschel, E. Goulielmakis, C. Gohle, R. Holzwarth, V. S. Yakovlev, A. Scrinzi, T. W. Hänsch, and F. Krausz, Nature (London) **421**, 611 (2003).

[23] T. Witting, F. Frank, W. A. Okell, C. A. Arrell, J. P. Marangos, and J. W. G. Tisch, J. Phys. B: At., Mol. Opt. Phys. **45**, 074014 (2012).

[24] M. J. Abel, T. Pfeifer, P. M. Nagel, W. Boutu, M. J. Bell, C. P. Steiner, D. M. Neumark, and S. R. Leone, Chem. Phys. **366**, 9 (2009).

[25] F. Ferrari, F. Calegari, M. Lucchini, C. Vozzi, S. Stagira, G. Sansone, and M. Nisoli, Nat. Photonics **4**, 875 (2010).

[26] I. J. Sola, E. Mével, L. Elouga, E. Constant, V. Strelkov, L. Poletto, P. Villoresi, E. Benedetti, J.-P. Caumes, S. Stagira, C. Vozzi, G. Sansone, and M. Nisoli, Nat. Phys. **2**, 319 (2006).

[27] Y. Mairesse and F. Quéré, Phys. Rev. A **71**, 011401(R) (2005).

[28] M. Lucchini, M. Brügmann, A. Ludwig, L. Gallmann, U. Keller, and T. Feurer, Opt. Express **23**, 29502 (2015).

[29] K. T. Kim, C. Zhang, A. D. Shiner, B. E. Schmidt, F. Légaré, D. M. Villeneuve, and P. B. Corkum, Nat. Photonics **7**, 958 (2013).

[30] P. Carpeggiani, M. Reduzzi, A. Comby, H. Ahmadi, S. Kühn, F. Calegari, M. Nisoli, F. Frassetto, L. Poletto, D. Hoff, J. Ullrich, C. D. Schröter, R. Moshammer, G. G. Paulus, and G. Sansone, Nat. Photonics **11**, 383 (2017).

[31] H. Wang, M. Chini, S. D. Khan, S. Chen, S. Gilbertson, X. Feng, H. Mashiko, and Z. Chang, J. Phys. B: At., Mol. Opt. Phys. **42**, 134007 (2009).

[32] F. Krausz and M. I. Stockman, Nat. Photonics **8**, 205 (2014).

[33] M. Chini, K. Zhao, and Z. Chang, Nat. Photonics **8**, 178 (2014).

[34] Y. Huismans, A. Rouzée, A. Gijsbertsen, J. H. Jungmann, A. S. Smolkowska, P. S. W. M. Logman, F. Lépine, C. Cauchy, S. Zamith, T. Marchenko, J. M. Bakker, G. Berden, B. Redlich, A. F. G. van der Meer, H. G. Muller, W. Vermin, K. J. Schafer, M. Spanner, M. Y. Ivanov, O. Smirnova *et al.*, Science **331**, 61 (2011).

[35] P. B. Corkum, Phys. Rev. Lett. **71**, 1994 (1993).

[36] Q. Z. Xia, J. F. Tao, J. Cai, L. B. Fu, and J. Liu, Phys. Rev. Lett. **121**, 143201 (2018).

[37] J. Cai, Y.-j. Chen, Q.-z. Xia, D.-f. Ye, J. Liu, and L.-b. Fu, Phys. Rev. A **96**, 033413 (2017).

[38] M. Li, H. Xie, W. Cao, S. Luo, J. Tan, Y. Feng, B. Du, W. Zhang, Y. Li, Q. Zhang, P. Lan, Y. Zhou, and P. Lu, Phys. Rev. Lett. **122**, 183202 (2019).

[39] S. Brennecke and M. Lein, Phys. Rev. A **100**, 023413 (2019).

[40] J. Liu, *Classical Trajectory Perspective of Atomic Ionization in Strong Laser Fields* (Springer-Verlag, Berlin, 2014).

[41] J. Daněk, K. Z. Hatsagortsyan, and C. H. Keitel, Phys. Rev. A **97**, 063409 (2018).

[42] K. W. Ford and J. A. Wheeler, Ann. Phys. **7**, 259 (1959).

[43] S. D. López and D. G. Arbó, Phys. Rev. A **100**, 023419 (2019).

[44] J. F. Tao, Q. Z. Xia, J. Cai, L. B. Fu, and J. Liu, Phys. Rev. A **95**, 011402(R) (2017).

[45] A. Ludwig, J. Maurer, B. W. Mayer, C. R. Phillips, L. Gallmann, and U. Keller, Phys. Rev. Lett. **113**, 243001 (2014).

[46] M.-X. Wang, H. Liang, X.-R. Xiao, S.-G. Chen, W.-C. Jiang, and L.-Y. Peng, Phys. Rev. A **98**, 023412 (2018).

[47] P.-L. He, D. Lao, and F. He, Phys. Rev. Lett. **118**, 163203 (2017).

[48] A. Hartung, S. Eckart, S. Brennecke, J. Rist, D. Trabert, K. Fehre, M. Richter, H. Sann, S. Zeller, K. Henrichs, G. Kastirke, J. Hoehl, A. Kalinin, M. S. Schöffler, T. Jahnke, L. P. H. Schmidt, M. Lein, M. Kunitski, and R. Dörner, Nat. Phys. **15**, 1222 (2019).

[49] M. Kübel, G. P. Katsoulis, Z. Dube, A. Y. Naumov, D. M. Villeneuve, P. B. Corkum, A. Staudte, and A. Emmanouilidou, Phys. Rev. A **100**, 043410 (2019).

[50] C. T. L. Smeenk, L. Arissian, B. Zhou, A. Mysyrowicz, D. M. Villeneuve, A. Staudte, and P. B. Corkum, Phys. Rev. Lett. **106**, 193002 (2011).

[51] X.-M. Tong and S.-I. Chu, Chem. Phys. **217**, 119 (1997).

[52] H. R. Reiss, Phys. Rev. Lett. **101**, 043002 (2008).

[53] X. M. Tong, K. Hino, and N. Toshima, Phys. Rev. A **74**, 031405(R) (2006).

[54] X.-M. Tong, J. Phys. B: At. Mol. Opt. Phys. **50**, 144004 (2017).

[55] G. Duchateau, E. Cormier, H. Bachau, and R. Gayet, Phys. Rev. A **63**, 053411 (2001).

[56] G. Duchateau, E. Cormier, and R. Gayet, Phys. Rev. A **66**, 023412 (2002).

[57] D. G. Arbó, J. E. Miraglia, M. S. Gravielle, K. Schiessl, E. Persson, and J. Burgdörfer, Phys. Rev. A **77**, 013401 (2008).

[58] L.-Y. Peng and Q. Gong, Comput. Phys. Commum. **181**, 2098 (2010).

[59] J. Tan, Y. Zhou, M. He, Y. Chen, Q. Ke, J. Liang, X. Zhu, M. Li, and P. Lu, Phys. Rev. Lett. **121**, 253203 (2018).

[60] J. Tross, G. Kolliopoulos, and C. A. Trallero-Herrero, Opt. Express **27**, 22960 (2019).

[61] B. HuP, J. Liu, and S. Gang Chen, Phys. Lett. A **236**, 533 (1997).

[62] N. B. Delone and V. P. Krainov, J. Opt. Soc. Am. B **8**, 1207 (1991).

[63] A. Kästner, U. Saalmann, and J. M. Rost, Phys. Rev. Lett. **108**, 033201 (2012).

[64] J. Daněk, M. Klaiber, K. Z. Hatsagortsyan, C. H. Keitel, B. Willenberg, J. Maurer, B. W. Mayer, C. R. Phillips, L. Gallmann, and U. Keller, J. Phys. B: At., Mol. Opt. Phys. **51**, 114001 (2018).

[65] M. Klaiber, K. Z. Hatsagortsyan, J. Wu, S. S. Luo, P. Grugan, and B. C. Walker, Phys. Rev. Lett. **118**, 093001 (2017).

[66] L. Keldysh, Zh. Eksp. Teor. Fiz. **47**, 1945 (1964) [Sov. Phys. JETP **20**, 1307 (1965)].

[67] A. Poppe, R. Holzwarth, A. Apolonski, G. Tempea, C. Spielmann, T. Hänsch, and F. Krausz, Appl. Phys. B **72**, 373 (2001).

[68] V. Strelkov, A. Zaïr, O. Tcherbakoff, R. López-Martens, E. Cormier, E. Mével, and E. Constant, J. Phys. B: At., Mol. Opt. Phys. **38**, L161 (2005).

[69] H. Mashiko, S. Gilbertson, C. Li, S. D. Khan, M. M. Shakya, E. Moon, and Z. Chang, Phys. Rev. Lett. **100**, 103906 (2008).

[70] P. Eckle, M. Smolarski, P. Schlup, J. Biegert, A. Staudte, M. Schöffler, H. G. Muller, R. Dörner, and U. Keller, Nat. Phys. **4**, 565 (2008).

[71] R. Kienberger, E. Goulielmakis, M. Uiberacker, A. Baltuska, V. Yakovlev, F. Bammer, A. Scrinzi, T. Westerwalbesloh, U. Kleineberg, U. Heinzmann, M. Drescher, and F. Krausz, Nature (London) **427**, 817 (2004).

[72] M. Richter, M. Kunitski, M. Schöffler, T. Jahnke, L. P. H. Schmidt, and R. Dörner, Phys. Rev. A **94**, 033416 (2016).

[73] D. Azoury, O. Kneller, S. Rozen, B. D. Bruner, A. Clergerie, Y. Mairesse, B. Fabre, B. Pons, N. Dudovich, and M. Krüger, Nat. Photonics **13**, 54 (2019).